SHIH-HSIEN CHANG©[1*], KUN-JIE LIAO©[1], KUO-TSUNG HUANG©[2], CHENG LIANG©[1]

EFFECTS OF THE MICROSTRUCTURE AND STRENGTHENING MECHANISMS OF MO₂C POWDERS BEING ADDED TO Ti-8Nb-4Co ALLOY *VIA* THE VACUUM SINTERING PROCESS

This study utilizes Ti-8Nb-4Co alloys added to different proportions of Mo_2C powders (1, 3, and 5 mass%) by the vacuum sintering process of powder metallurgy and simultaneously vacuum sinters the alloys at 1240, 1270, 1300, and 1330°C for 1 h, respectively. The experimental results indicate that when 3 mass% Mo_2C powders were added to the Ti-8Nb-4Co alloys, the specimens possessed the optimal mechanical properties after sintering at 1300°C for 1 h. The relative density was 98.02%, and the hardness and TRS were enhanced to 69.6 HRA and 1816.7 MPa, respectively. In addition, the microstructure of vacuum sintered Ti-8Nb-4Co-3Mo_2C alloys has both α and β-phase structures, as well as TiC precipitates. EBSD results confirm that the Mo_2C in situ produced TiC during the sintering process and was uniformly dispersed in the grain boundary. Moreover, the reduced molybdenum atom acted as a β-phase stabilizing element and solid-solution in the titanium matrix.

Keywords: Ti-8Nb-4Co alloy; Mo_2C powders; vacuum sintering; TRS; EBSD

1. Introduction

Due to their high specific strength, excellent corrosion resistance, good biocompatibility, and low elastic modulus, titanium (Ti) alloys are commonly used in automotive and aerospace industries, as well as in biomedical materials [1-3]. It is well known that the high cost of Ti, both in terms of extraction and manufacturing, is the main limiting factor for the widespread use of Ti industry [4,5]. Furthermore, by adding β-stabilizing elements such as niobium (Nb), tantalum (Ta), molybdenum (Mo), the high-temperature β-phase of Ti alloys can be stabilized. Among them, Nb is reported as favorable for osteogenesis, cell adhesion and proliferation [6]. Hence, Ti-Nb-based alloys are considered materials for orthopedic implants due to their excellent biocompatibility, low elastic modulus and good superelastic properties [7,8].

Compared with the traditional Ti alloys, the addition of cobalt (Co) usually affects the sintering temperature (the melting range of the Ti-Co alloy is about 1062-1088°C, which is 568°C lower than that of Ti) [9]. In addition, Co alloy is widely used in biomedical implants, especially in total hip and knee replacements and dental devices, due to its good biocompatibility, indicating that Co is harmless to the body. Co is a good adding element in Ti alloys as biomaterials [9]. In fact, the Ti-Co-based biomaterials have become a hot topic in the past year. Literature indicates that the Ti-based alloys with cobalt addition show higher strength and lower melting temperature. It is worth mentioning that the addition of Co improves the corrosion resistance of titanium and its mechanical properties [10,11].

Metal matrix composites (MMCs) have advantages over alloys such as better wear resistance, a low thermal expansion coefficient, and good mechanical properties at elevated temperatures. These materials combine a soft metallic matrix with hard ceramic particles that with stand wear. In general, the strengthening in alloys is attributed to the presence of intermetallic; however, in the case of MMCs, it is attributed to the presence of reinforcement [12]. Furthermore, additions of carbides such as NbC, HfC, VC, ZrC, Mo_2C, TiB_2, TaC or TiC to the powder mixtures are often done in order to increase the wear resistance for high-speed machining operations of steel. These carbides are known to inhibit grain growth in high-temperature sintering in the powder metallurgy (PM) process [13,14]. Among these carbides, molybdenum carbide (Mo_2C) has received considerable attention as a refractory hard material because it offers attractive properties such as high hardness, high melting point, and high chemical stability. It has been widely applied as a reinforcement

[1] NATIONAL TAIPEI UNIVERSITY OF TECHNOLOGY, DEPARTMENT OF MATERIALS AND MINERAL RESOURCES ENGINEERING, TAIPEI 10608, TAIWAN, ROC
[2] NATIONAL KANGSHAN AGRICULTURAL INDUSTRIAL SENIOR HIGH SCHOOL, DEPARTMENT OF AUTO-MECHANICS, KAOHSIUNG 82049, TAIWAN, ROC

* Corresponding author: changsh@ntut.edu.tw

material in metal ceramics [15,16]. Moreover, Mo_2C is also the most effective grain growth inhibitor due to its excellent solubility and mobility in the metal matrix phase during the liquid phase sintering (LPS) of the PM process [17,18].

Previously, casting and subsequent thermomechanical treatment were often used to prepare Ti alloys; however, this has been replaced by the PM technique, which provides great opportunities for the development and production of high-performance Ti alloys at a lower cost. Furthermore, the addition of Mo_2C can form titanium matrix composites (TMCs), which enhance the mechanical properties of Ti alloys and can be used as a β-stabilizing element solid-solution in the titanium matrix, which causes the ductility to increase. As previously mentioned, while Ti-Nb alloys possess superior properties and have recently been widely researched by E. Yılmaz and A. Gökçe et al. [19-21], Ti-Nb-Co alloys have not been further studied or reported. Moreover, research on Ti-Nb-Co-xMo_2C titanium-based composites is even rarer. In order to improve the mechanical and corrosion properties of Ti-Nb-Co alloys while exploring the strengthening effect of Mo_2C. Therefore, this experiment used the vacuum sintering process of PM to prepare Ti-Nb-Co alloys, where Mo_2C was utilized as the strengthening phase additive, which was intended to achieve the purpose of strengthening the Ti-Nb-Co alloys.

2. Experimental procedures

In the first part of this study, three different powders (Ti, Nb, and Co) were uniformly mixed and used to produce three different proportions of Ti-Nb-Co alloys: Ti-8Nb-2Co, Ti-8Nb-4Co, and Ti-8Nb-6Co alloys. Moreover, the Ti-Nb-Co alloys underwent a vacuum sintering process at the sintering temperatures of 1200, 1225, 1250, and 1275°C for 1 h. The experimental results show that the Ti-8Nb-4Co alloys sintered at 1250°C for 1 h had better mechanical properties, where the relative density reached 97.35% and the hardness and TRS reached 67.9 HRA and 1715.7 MPa, respectively. In order to further improve the sintering density and properties of the Ti-8Nb-4Co alloys, this study utilized Ti-8Nb-4Co alloy powders and added different ratios of refined Mo_2C powders (1, 3, and 5 mass%) as a strengthening element to explore the effects of a series of vacuum sintering processes.

In this study, the mean particle sizes of Ti, Nb, Co, and Mo_2C powders were about 23.5±1.5, 17.1±0.5, 3.16±0.5, and 6.6±0.5 μm, respectively. While the morphology of the Ti and Nb powders presented an irregularly shaped surface, the Co powders possessed a nearly round appearance, and Mo_2C showed an irregularly shaped and polygonal appearance. Additionally, the different amounts of Mo_2C powder (1, 3, and 5 mass%) were mixed and added to Ti-8Nb-4Co alloy powders, hereafter, designated as 1 Mo_2C, 3 Mo_2C, and 5 Mo_2C. The mixing experiment utilized a three-degree space rotary mixer (Turbula Shaker-Mixer, T_2C). Meanwhile, the time of mixing was 24 hours, and the ratio of powder, stain remover oil and zirconia ball was 1:1:0.1, respectively. After milling, PVA (polyvinyl

alcohol) was added as a binder, and the powders compressed into rectangular-shaped green bodies ($40 \times 6 \times 6$ mm^3) under uniaxial pressure at 350 MPa for 300 s (specimens have also been examined and confirmed for the influence of the time of mixing on the uniformity of the powder mixture constituents distribution). Subsequently, the specimens were immediately vacuum sintered at 1240, 1270, 1300, and 1330°C for 1 h, respectively.

To evaluate the effects of microstructure evolution on the Mo_2C powders added to Ti-8Nb-4Co alloys, this study conducted volume shrinkage, apparent porosity, relative density, mean grain size, hardness, TRS tests, XRD (Bruker/D2 Phaser) analysis, Optical Microscopy (OM, Nikon optiphot 66), Scanning Electron Microscopy (SEM, Hitachi-S4700) and Electron Backscatter Diffraction (EBSD, JSM-7800F) microstructure observations. A porosity test was conducted in accordance with the ASTM C373-88 standard. Hardness tests were measured by HRA with a loading of 588 N, which followed the ASTM E18-3 standard. Furthermore, the Hung Ta universal material test machine (HT-9501A) with a maximum load of 25 tons was used for TRS tests (ASTM B528-05). The TRS was obtained by the equation $R_{bm} = 3FLk/2bh^2$, where R_{bm} is the TRS, which is determined as the fracture stress in the surface zone, and F is maximum fracture load. In this work, L was 30 mm, k was chamfer correction factor (normally 1.00-1.02), and b and h were 5 mm, respectively. The specimen dimensions for the TRS test were $5 \times 5 \times 40$ mm^3, and it tested at least three pieces.

In this study, corrosion potential (Potential Stat Chi 601) analysis uses three electrodes and follows by ASTM G59-97: the reference electrode is a saturated of silver-silver chloride electrode, the auxiliary electrode uses a platinum electrode, and the working electrode is connected to the test specimens [13,17]. The contact area of the specimen was 0.78 cm^2. The corrosive solvent used 1 N H_2SO_4 was maintained at room temperature. A scanning speed of 0.01 V·s^{-1}, an initial potential of –1.5 V, and the final potential of 3.5 V were controlled. The polarization curve was obtained by Corr-View software to analyze and compare the corrosion current (I_{corr}), corrosion potential (E_{corr}) and polarization resistance (R_p) of sintered Ti-8Nb-4Co-xMo_2C composite materials.

3. Results and discussion

3.1. Effect of Mo_2C content and sintering temperature on the mechanical properties

Fig. 1 displays the volume shrinkage, apparent porosity, and relative density of the various mass% Mo_2C added to Ti-8Nb-4Co alloys under the different sintering temperatures, and the results show that the volume shrinkage increased gradually (Fig. 1a) as the Mo_2C content ($1 \rightarrow 3 \rightarrow 5$ mass%) or the sintering temperature were increased ($1240 \rightarrow 1270 \rightarrow 1300 \rightarrow 1330°C$). When the sintering temperature reached 1330°C, due to the sufficiently high-temperature driving force, all of the specimens had relatively high-volume shrinkage (compared with

other relatively low sintering temperatures); among them, the 5 Mo$_2$C specimens sintered at 1330°C for 1 h possessed the highest volume shrinkage (35.42%). Whereas, the volume shrinkage of the 1 Mo$_2$C and 3 Mo$_2$C specimens after sintering at 1330°C was 33.85% and 34.88%, respectively. It is speculated that the Mo$_2$C additive had a relatively large elastic modulus (535 GPa), as indicated by the high rigidity, and thus required greater stress to produce the plastic deformation of the Ti-8Nb-4Co-xMo$_2$C alloys. However, as the forming pressure used in this experiment was only 350 MPa, the volume shrinkage rate of the specimens was relatively low after sintering. Furthermore, when 5 mass% Mo$_2$C was added, all volume shrinkage was slightly larger than 1 and 3 mass% after the different sintering temperatures. As the sintering temperature was increased, the volume shrinkage of all specimens had a tendency to increase significantly. Apparently, an increased Mo$_2$C content or sintering temperature effectively improved the volume shrinkage in this study.
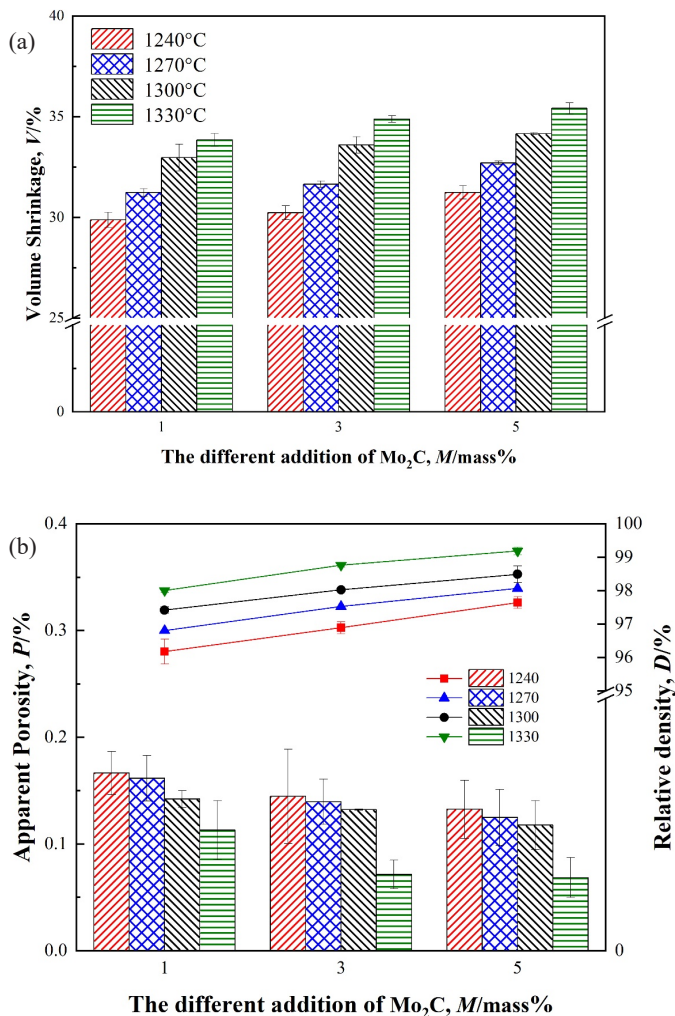

Fig. 1. Comparison of the (a) volume shrinkage, and (b) apparent porosity and relative density of various mass% Mo$_2$C added to Ti-8Nb-4Co alloys by the different sintering temperatures

Fig. 1b presents the apparent porosity of 1 Mo$_2$C, 3 Mo$_2$C, and 5 Mo$_2$C specimens after the different sintering temperatures for 1 h, and the results show that the apparent porosity of all

the specimens tended to significantly decrease as the sintering temperature increased. In this study, due to the addition of high-melting ceramic carbides (the melting point of Mo$_2$C is 2690°C), the driving force for sintering at 1240°C was insufficient; thus, when more Mo$_2$C was added, it easily led to increased remaining pores. As seen in Fig. 1b, the apparent porosity of all specimens was highest after sintering at 1240°C for 1 h, and when the sintering temperature was increased to 1270°C, the porosity declined slightly. When the sintering temperature was further enhanced to 1300°C, the apparent porosity gradually decreased with the increase in Mo$_2$C content. The apparent porosities of the 1 Mo$_2$C, 3 Mo$_2$C, and 5 Mo$_2$C specimens were 0.14%, 0.13%, and 0.12% after sintering at 1300°C, respectively; notably, when the sintering temperature exceeded 1300°C, the apparent porosity rapidly decreased. As previously stated, Mo$_2$C possessed excellent solubility and mobility in the high-temperature sintering process [17,18], which thereby enhanced the compactness of sintering. Obviously, the increase in the sintering temperature and additional amount of Mo$_2$C effectively reduced the apparent porosity, which is beneficial to sintering densification. Hence, the 3 Mo$_2$C and 5 Mo$_2$C specimens possessed the lowest apparent porosity (both are 0.07%) after 1330°C sintering for 1 h. Literature indicates that an increase in sintering temperature can enhance thermal energy [13,14], and this article further confirms that increasing the sintering temperature is effective in increasing the driving force for Ti-8Nb-4Co-xMo$_2$C alloys, thereby reducing the porosity.

The relative densities of the 1 Mo$_2$C, 3 Mo$_2$C, and 5 Mo$_2$C specimens after the different sintering temperatures for 1 h are also shown in Fig. 1b. The relative density has an opposite trend to the apparent porosity. As stated earlier, the Ti-8Nb-4Co-xMo$_2$C specimens require a higher temperature to achieve complete densification; thus, when the sintering temperature was increased to 1300°C, the relative density was significantly increased. Moreover, all the specimens had higher relative density than that of the Ti-8Nb-4Co alloys (97.35%), which shows that adding Mo$_2$C to the Ti-8Nb-4Co alloy in the sintering range of 1300°C~1330°C is effective in improving sintering densification. In this work, while the 5 Mo$_2$C specimens sintered at 1330°C possessed the highest relative density (99.19%); simultaneously, the 3 Mo$_2$C specimens also had a good relative density (98.76%) after sintering at 1330°C. The porosity values of the 3 Mo$_2$C and 5 Mo$_2$C specimens were almost less than 1% after sintering at 1330°C, respectively, which means that the near-full theoretical sintered density of the Ti-8Nb-4Co-xMo$_2$C alloys can be acquired. According to the above discussion and results, the addition of Mo$_2$C not only enhanced the volume shrinkage of Ti-8Nb-4Co-xMo$_2$C alloys but also improved the relative density and apparent porosity by adding the appropriate content of Mo$_2$C.

Fig. 2 shows the hardness and TRS test results of various mass% Mo$_2$C added to Ti-8Nb-4Co alloys for the different sintering temperatures. The hardness values of the Ti-8Nb-4Co-xMo$_2$C specimens were obviously enhanced as the amount of added Mo$_2$C was increased. Moreover, the hardness dramatically

increased as the sintering temperature was increased. Generally speaking, decreasing the porosity and increasing the density of sintered materials could effectively enhance plastic deformation resistance and hardness [11,13,14]. Compared with the hardness of the Ti-8Nb-4Co alloys (67.9 HRA), the specimens with added Mo$_2$C had obviously increased hardness, as shown in Fig. 2a. It was found that when various mass% Mo$_2$C were added to Ti-8Nb-4Co alloys, the hardness visibly increased after 1300 and 1330°C sintering for 1 h. As mentioned earlier in this paper, Mo can be used as a β-stabilizing element for forming a homogeneous solid-solution in the titanium matrix, which results in a strengthening effect. Apparently, Mo$_2$C had a significant strengthening effect on Ti-8Nb-4Co alloys. It is possible to say that the solid-solution of Mo increased the stability of the β-phase, thus, forming more ductile β-phases. At the same time, the in situ reaction (Mo$_2$C + Ti → 2Mo + TiC) produced a large amount of TiC (this inference is confirmed in the subsequent EBSD analysis), which precipitates in the grain boundaries and can effectively prevent dislocation movement to achieve dispersion strengthening effects. Consequently, the 5 Mo$_2$C specimens

had the highest hardness (71.0 HRA) after 1330°C sintering for 1 h. Moreover, the 1 Mo$_2$C and 3 Mo$_2$C specimens also had good hardness after 1330°C sintering for 1 h, with hardness values of 69.2 and 70.4 HRA, respectively.

Fig. 2b shows the TRS values of Ti-8Nb-4Co-xMo$_2$C specimens after various sintering temperatures. It is worth noting that the TRS value of Ti-8Nb-4Co-xMo$_2$C specimens had a tendency to first rise, and then, decline as the sintering temperature was increased. Mo$_2$C and Ti will produce in situ reaction to generate Mo and TiC atoms (Mo$_2$C + Ti → 2Mo + TiC). Among them, Mo is a β-stabilizing element that can effectively strengthen the properties of Ti alloys and has the effects of solid-solution strengthening and grain refinement [18]. In addition, an appropriate amount of TiC produced by in situ reactions will effectively improve the strength of Ti alloys, thus, the solid-solution of Mo and the in situ reaction of TiC have the effect of greatly improving strength. As the sintering temperature was increased the porosities decreased (as seen in Fig. 1b), while the amount of carbide precipitates increased, thus, the strength rapidly increased. Moreover, when the sintering temperature was increased to 1300°C, it was observed that the TRS of all the specimens reached the highest values. The TRS values of 1 Mo$_2$C, 3 Mo$_2$C, and 5 Mo$_2$C samples were 1748.9, 1816.7, and 1453.4 MPa after being sintered at 1300°C for 1 h, respectively. It can be reasonably concluded that, since the solid-solution reaction of the Mo elements appeared in the Ti-8Nb-4Co-xMo$_2$C specimens, they possessed lower apparent porosity, more β-phase fractions, a large amount of precipitated carbides, and inhibited grain growth, thus, all the 1300°C sintered- Ti-8Nb-4Co-xMo$_2$C specimens had the highest TRS values.

However, due to the high temperature of grain growth, the TRS values of all the specimens obviously declined. In this study, the mean grain sizes of the 1 Mo$_2$C, 3 Mo$_2$C, and 5 Mo$_2$C specimens were 79.28, 74.31, and 67.47 μm after being sintered at 1330°C for 1 h, respectively, which led to reduced TRS values. It was speculated that, in addition to excessive grain growth, the content of precipitated carbides also increased, which resulted in excessive hard and brittle strengthening phases in the matrix and a significant decline in the TRS values. According to the Hall-Petch equation of the fine-grain strengthening theory, the change in grain size will affect the mechanical properties of alloy materials [22,23]. Consequently, no obvious grain coarsening appeared in the 1300°C sintered- 3 Mo$_2$C samples (59.27 μm), which resulted in the highest TRS value. In addition, at the same sintering temperature, the mean grain size after adding 5 mass% Mo$_2$C was smaller than that of 1 and 3 mass%, which confirms that adding Mo$_2$C has an obvious effect on inhibiting grain growth. Therefore, adding an appropriate amount of Mo$_2$C powders to Ti-8Nb-4Co alloys is effective in improving their mechanical properties after the vacuum sintering process. In this experiment, the 1300°C sintered- 3 Mo$_2$C specimens possessed the ideal hardness (69.6 HRA) and the highest TRS value (1816.7 MPa), which are better than those of the Ti-8Nb-4Co alloy (whose hardness is 67.9 HRA and TRS value is 1715.7 MPa).
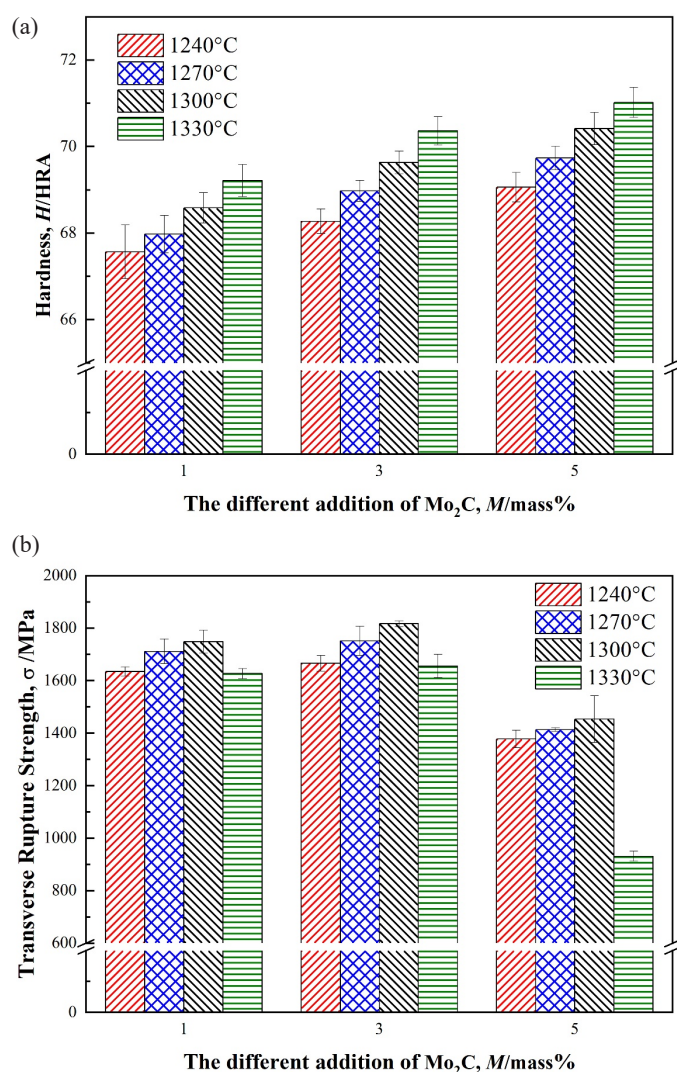

Fig. 2. Comparison of the hardness and TRS of various mass% Mo$_2$C added to Ti-8Nb-4Co alloys after sintering at different temperatures for 1 h: (a) hardness, and (b) TRS

According to the above discussion and results, it is reasonable to conclude that the 1300°C sintered- 3 Mo₂C specimens have the optimal sintering characteristics and mechanical properties. The follow-up experiments will conduct microstructure analysis and corrosion testing on the Ti-8Nb-4Co-xMo₂C specimens using a sample from the optimal sintering temperature (1300°C).

3.2. Effect of microstructure and corrosion behaviors on sintered Ti-8Nb-4Co-xMo₂C alloys

Fig. 3 displays the XRD patterns of various amounts of Mo₂C added to Ti-8Nb-4Co alloys after sintering at 1300°C for 1 h, and the results show that the main diffraction peaks are α-Ti, β-Ti, and TiC. It was observed that the peak of molybdenum carbide (Mo₂C, PDF#35-0787) had completely disappeared and was replaced by the titanium carbide peak (TiC, PDF#32-1383). Literature points out that the standard free energy of the formation of TiC is much lower than that of Mo₂C [24]. Thus, in situ, Mo₂C will decompose into carbon and molybdenum during the high-temperature sintering process. Among them, carbon reacts with titanium to form titanium carbide (Mo₂C + Ti → 2Mo + TiC), and molybdenum is a solid-solution in titanium as a β-phase stabilizing element. This result can be verified by the fact that the peak value of TiC will increase with the increase of Mo₂C, and it is confirmed that TiC is indeed transformed from Mo₂C. According to the above theory and discussions, Mo₂C added to the Ti-8Nb-4Co alloy plays an important role in generating TiC after sintering at 1300°C for 1 h. In addition, as Mo is the β-phase stabilizing element of Ti alloys, the solid-solution of Mo in the matrix material will make the Ti alloy produce a stable β-phase. Thus, it can also be observed that, with the increased Mo₂C amount (1 → 3 → 5 mass%), the peak value of the α phase will gradually decrease, while the peak value of the β-pha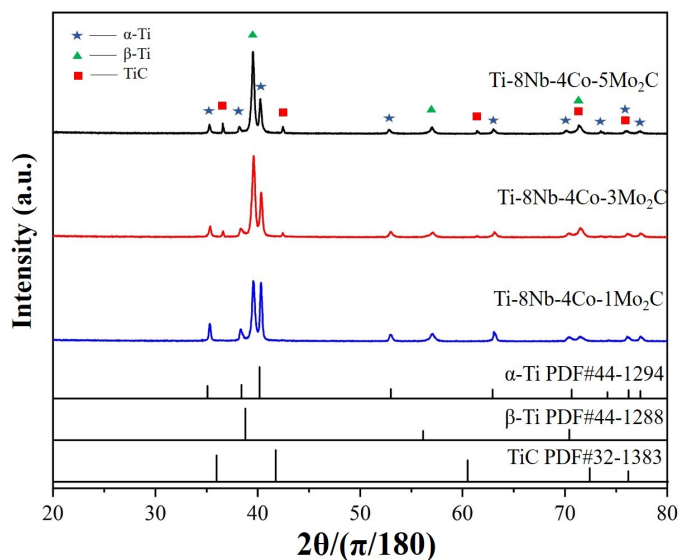se will significantly increase. In addition, the diffraction peak of the β-phase was simultaneously increased and shifted to higher angles, and the same trend can be observed at the sintering temperatures of 1240, 1270, and 1330°C.

Fig. 4 shows the OM images of various mass% Mo₂C added to Ti-8Nb-4Co alloys after sintering at 1300°C for 1 h. It was observed that there were many slender flaky α-phases with staggered distribution in the β-phase matrix as 1 mass% Mo₂C was added (Fig. 4a), while the discontinuous and coarse α-phase precipitated from the β grain boundaries. There was a refining phenomenon of grain size when the Mo₂C was increased to 3 mass%, as shown in Fig. 4b. Moreover, as the slender flaky α-phase gradually decreased, the α-phase in the β-phase matrix became less obvious. This result also supports the previous XRD analysis, meaning that the higher Mo₂C content will cause the diffraction peak of the β-phase to have stronger intensity, while the diffraction peak of the α-phase will have weaker intensity.

As the content of Mo₂C was increased to 5 mass%, more carbide particles were found to precipitate on the grain boundaries, as shown in Fig. 4c; notably, these carbides were mainly TiC precipitates. As stated earlier, in situ, Mo₂C will decompose into carbon and molybdenum during the high-temperature sintering process. As 1 mole of Mo₂C can reduce 2 moles of Mo, the more Mo₂C that is added (5 mass%), the more Mo that is reduced. In other terms, when more Mo₂C powders are added, the chance of an in situ reaction of Mo₂C increases significantly; therefore, as the content of Mo₂C increases, the content of the β-phase rapidly increases, and a greater amount of precipitation TiC can be seen on the grain boundaries. However, too many TiC carbide precipitates in the grain boundary do not help to improve the strength of the materials; thus, the TRS of the 5 Mo₂C specimens (Fig. 2b) was significantly lower than that of 1 Mo₂C and 3 Mo₂C after sintering at 1300°C for 1 h. According to the above OM observation, adding an appropriate content of Mo₂C (3 mass%) obviously helps to decrease the slender flaky α-phase, while increasing the β-phase and the appropriate amount of TiC precipitates, which is effective in improving the strength of the Ti-8Nb-4Co alloys. All the phase distributions of Ti-8Nb-4Co-3Mo₂C alloys were further examined by subsequent EBSD analysis.

Figs. 5a and 5b present the low-magnification and high-magnification SEM images of Ti-8Nb-4Co-3Mo₂C alloys after sintering at 1300°C for 1 h, respectively, while the EDS analysis results are listed in Table 1. In this work, the constituent elements of locations 5a-1 and 5b-1 are the solid-solution phases of Ti and Nb, respectively. It is reasonably speculated that the precipitates could be the slender flaky α-phase. Moreover, XRD analysis found that the intensity of the diffraction peak of the β-phase mainly depends on the content of Mo₂C. With the increased Mo₂C content, more molybdenum atoms were produced by the in situ reaction, and the intensity of the diffraction peak of the β-phase was increased (Fig. 3). As a result, locations 5a-2 and 5b-2 are composed of Ti, Nb, Co, and Mo elements, respectively. Since Mo is a β-phase stable element, it is reasonable to suggest that this precipitate is likely to be a β-phase.
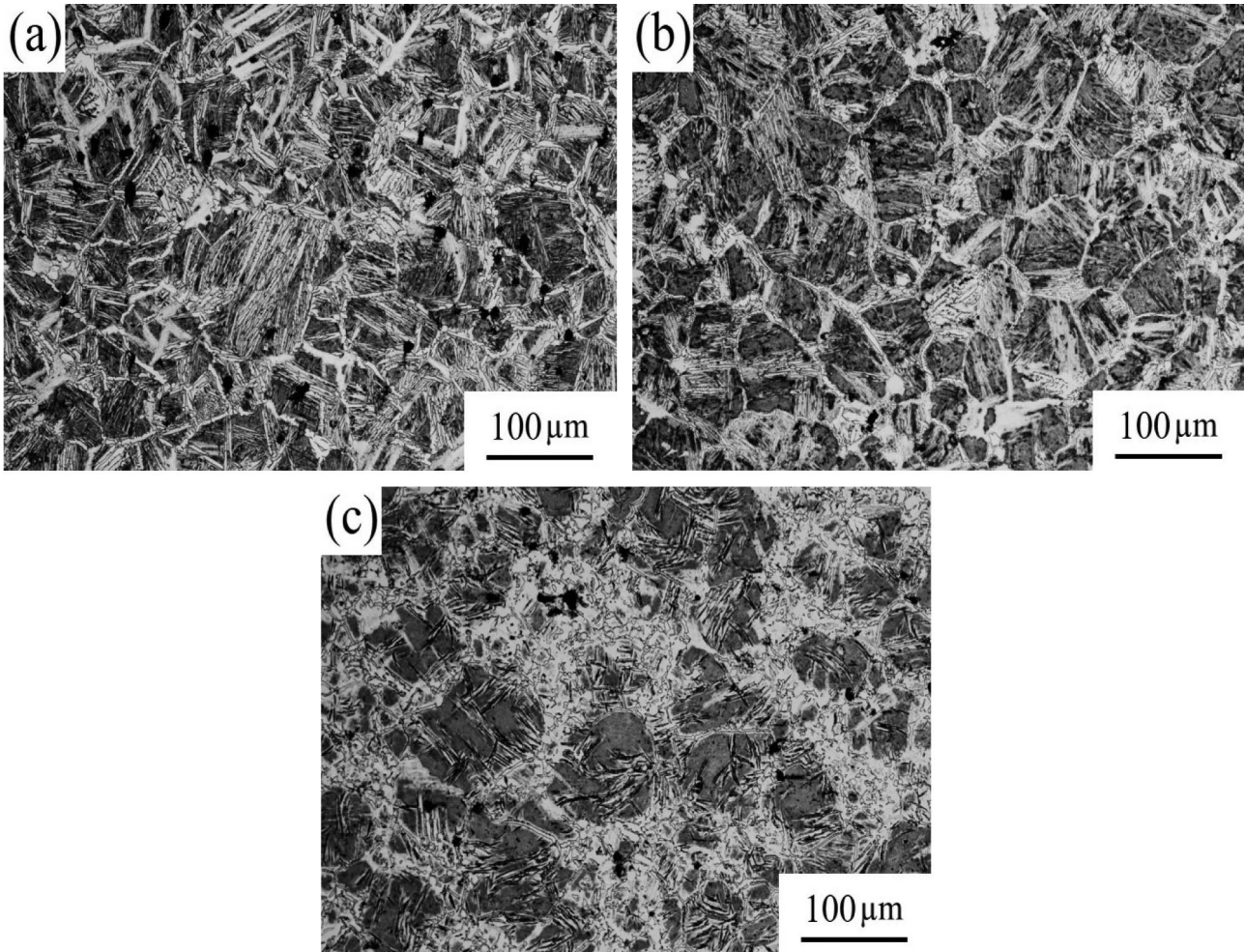

Fig. 3. XRD pattern of various mass% Mo₂C added to Ti-8Nb-4Co alloys after sintering at 1300°C for 1 h

Fig. 4. The OM images of various mass% Mo_2C added to Ti-8Nb-4Co alloys after sintering at 1300°C for 1 h. (a) 1 Mo_2C, (b) 3 Mo_2C, and (c) 5 Mo_2C

In addition, the compositions of locations 5a-3 and 5b-3 are Ti and C elements, respectively, as seen in TABLE 1. Among them, titanium accounts for 54.06 at% and carbon accounts for 45.94 at% (location 5a-3); thus, the composition ratio of the two elements is almost 1:1, and according to the preliminary judgment, the precipitates could be TiC. Furthermore, the com-positions of locations 5a-4 and 5b-4 are Ti, Nb, and C elements, respectively. It is worth noting that the carbon content was much higher than that of niobium; as shown in TABLE 1, where the niobium content is 1.28 at% and carbon content is 37.78 at% (location 5a-4), thus, the precipitates should be mainly TiC. Obviously, this finding agrees with the observed TiC in the previ-
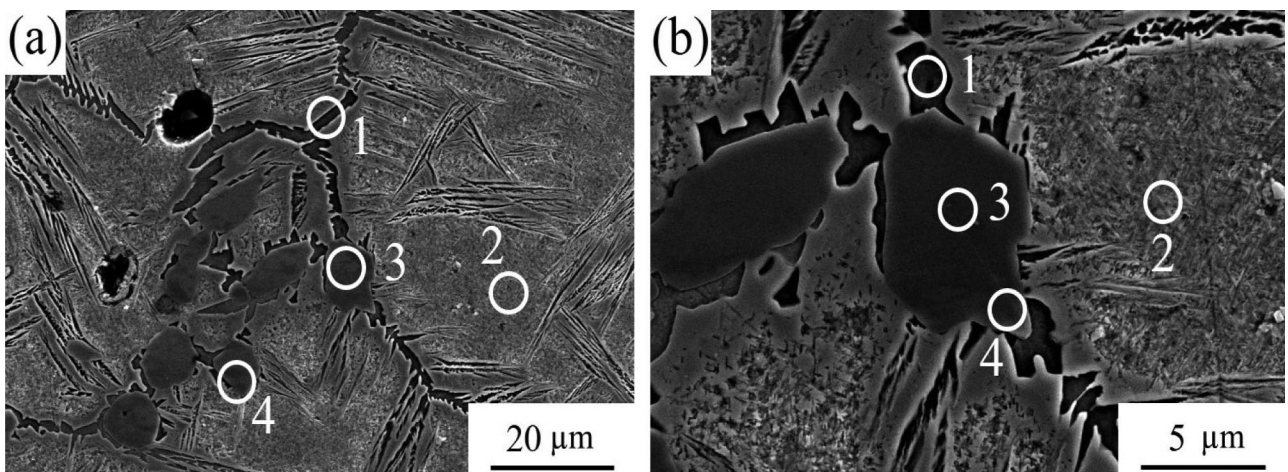

Fig. 5. The SEM images of Ti-8Nb-4Co-3Mo$_2$C alloys after sintering at 1300°C for 1 h: (a) low-magnification, and (b) high-magnification images

ous XRD analysis. Moreover, the EDS results also confirm the previous discussions of this paper, meaning the carbon indeed reacts with titanium to form titanium carbide and molybdenum is a solid solution in titanium as a β-phase stabilizing element. Subsequently, this study used EPMA to check the element distribution, while EBSD confirmed the existence of TiC precipitates.

TABLE 1

The EDS analysis of the Figs. 5a and 5b

Elements (at%)	(a)-1	(a)-2	(a)-3	(a)-4	(b)-1	(b)-2	(b)-3	(b)-4
Ti	97.11	87.25	54.06	60.94	97.15	86.75	54.55	60.82
Nb	2.89	4.93	—	1.28	2.85	5.02	—	1.31
Co	—	4.75	—			4.85	—	—
Mo	—	3.07	—			3.38	—	—
C	—	—	45.94	37.78		—	45.45	37.87

In addition to the mechanical properties of high strength and high hardness, titanium alloys must possess good corrosion resistance, in order to examine the corrosion resistance of Ti-8Nb-4Co-xMo$_2$C (x = 1, 3, 5 mass%) alloy in harsh environments. Fig. 6 displays the Tafel slope results of 1300°C sintered- 1 Mo$_2$C, 3 Mo$_2$C, and 5 Mo$_2$C specimens after 1 N H$_2$SO$_4$ corrosion testing. The experimental results show that all the specimens possessed a significant passivation phenomenon. Generally speaking, a passivation layer will be produced on the material's surface, which can effectively protect the interior material, thereby improving the corrosion resistance, and this result indicates that the sintered- Ti-8Nb-4Co-xMo$_2$C specimens have excellent corrosion resistance. This study uniformly dissolved both Nb and Mo elements in the titanium substrate, which are advantageous for improving corrosion resistance, while adding Nb, Co, and Mo elements to the Ti alloy can strengthen the passivation film of the Ti-based alloys [7,8,10,11].
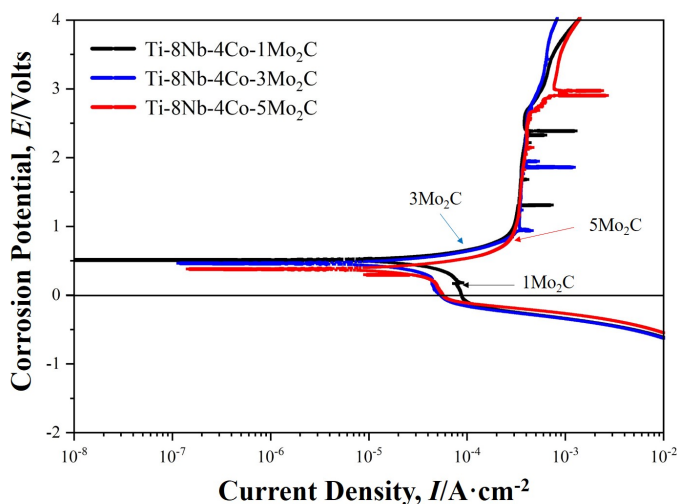

Fig. 6. Tafel results of various mass% Mo$_2$C added to Ti-8Nb-4Co alloys after sintering at 1300°C for 1 h

Although the Tafel slope result of the specimens did not display a significant variation (because there is not much difference between the corrosion data of the experimental specimens), the increase in the amount of Mo$_2$C led to a corrosion current decline and rise (5.62 → 4.11 → 4.84×10^{-5} A·cm^{-2}). This study also considered polarization resistance, as higher polarization resistance usually means better corrosion resistance [13,14]. As the added Mo$_2$C content was increased, the polarization resistance rose slightly and then declined (4.63 → 6.34 → 5.37×10^3 Ω·cm^2). In this study, the addition of 3 mass% Mo$_2$C had the highest polarization resistance value (6.34×10^3 Ω·cm^2), and it was speculated that the TiC content of 3 Mo$_2$C specimens was less than that of the 5 Mo$_2$C specimens after the in situ reaction. While the TiC strengthening phase can improve the mechanical properties of the materials, the greater the TiC content, the greater the probability of intergranular corrosion in the material; thus, the corrosion resistance of the 5 Mo$_2$C specimens was slightly reduced (5.37×10^3 Ω·cm^2). Consequently, the 3 Mo$_2$C specimens possessed the highest polarization resistance and lowest corrosion current values, indicating optimal corrosion resistance.

3.3. Effect of phase distribution and crystal orientation on sintered- Ti-8Nb-4Co-xMo$_2$C alloys

According to the above X-ray and microstructure analysis conducted in this paper, TiC precipitates appeared in the Ti-8Nb-4Co-xMo$_2$C alloy. In order to further judge whether or not the precipitates were TiC and to understand the phase distribution and crystal orientation in the Ti-8Nb-4Co-xMo$_2$C alloy, subsequent research used EBSD and EPMA analysis for the 1300°C sintered- Ti-8Nb-4Co-xMo$_2$C specimens.

Fig. 7 shows the phase distribution of the EBSD analysis for various mass% Mo$_2$C added to Ti-8Nb-4Co alloys after sintering at 1300°C for 1 h. Figs. 7a, 7c, and 7e show the image quality of the 1 Mo$_2$C, 3 Mo$_2$C, and 5 Mo$_2$C specimens, respectively, while Figs. 7b, 7d, and 7f show the phase mapping of the 1 Mo$_2$C, 3 Mo$_2$C, and 5 Mo$_2$C specimens, respectively. The EBSD analysis results clearly display the α-phase (the red part of Fig. 7b), the β-phase (the blue part of Fig. 7b), and the TiC phase (the yellow part of Fig. 7d) in the 1300°C sintered- Ti-8Nb-4Co-xMo$_2$C alloys. It can be found that the 1 Mo$_2$C specimen had almost no TiC phase signal (Fig. 7b). It is reasonable to surmise that when 1 mass% Mo$_2$C was added, the amount of added Mo$_2$C was insufficient, and thus the result in the TiC phase could not be completely precipitated on the grain boundary. Notably, with the increase of Mo$_2$C content, the proportion of β-phase and TiC phase gradually increased. At the same time, the signal with the TiC structure (yellow part) can be observed more clearly from Figs. 7d and 7f. This finding is consistent with previous XRD and EDS analysis results. It can be further confirmed that TiC is indeed precipitated in Ti-8Nb-4Co-xMo$_2$C alloy after being sintered at 1300°C for 1 h.

In addition, the results of the EBSD analysis of the structure distribution ratio for various mass% Mo$_2$C added to Ti-8Nb-4Co alloys after sintering at 1300°C for 1 h are shown in TABLE 2,
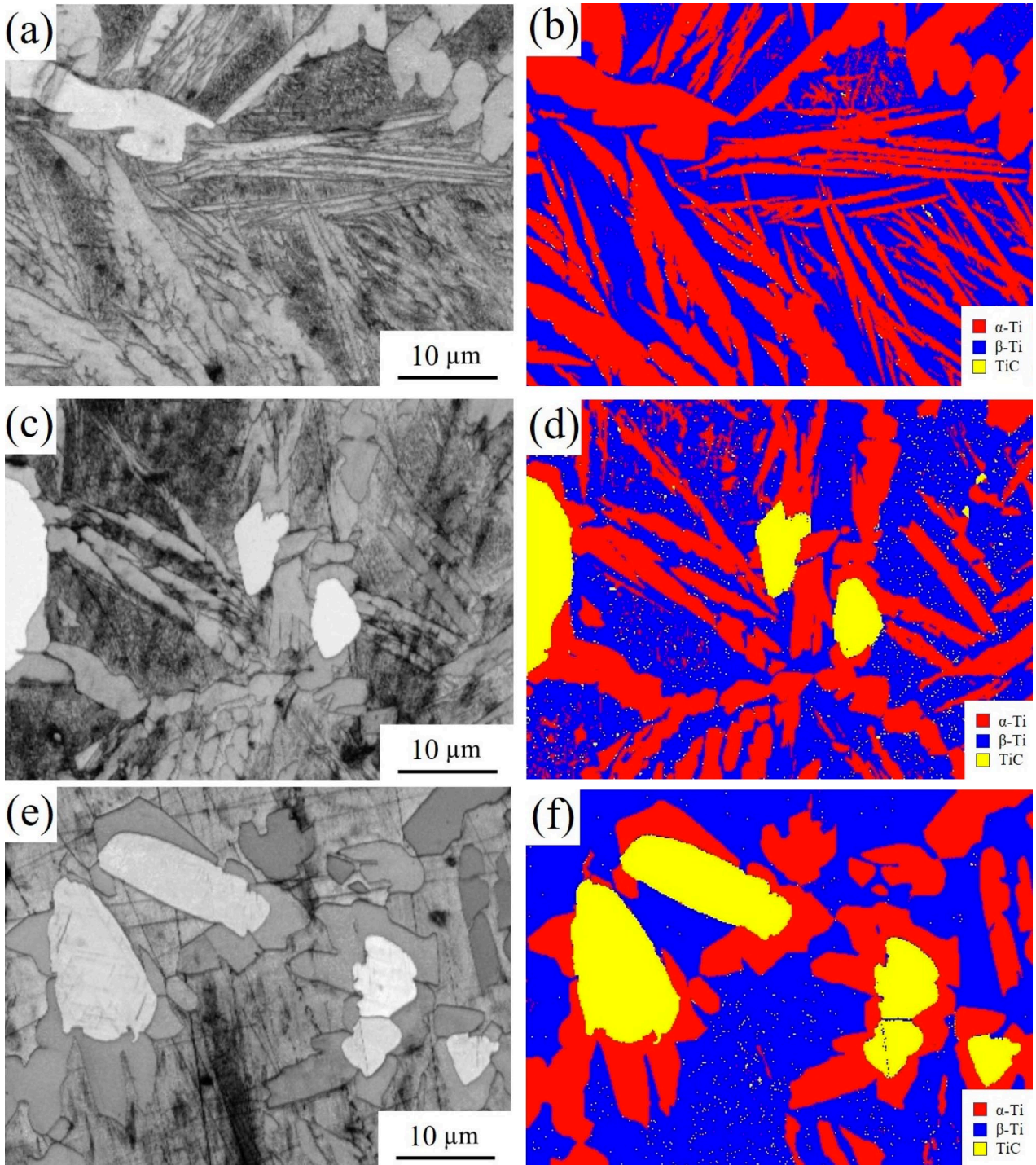
Fig. 7. The EBSD analysis for various mass% Mo$_2$C added to Ti-8Nb-4Co alloys after sintering at 1300°C for 1 h: (a), (c), (e) image quality, (b), (d) and (f) phase mapping, which are1 Mo$_2$C, 3 Mo$_2$C and 5 Mo$_2$C, respectively

where zero is the position distribution ratio of no signal in the image. Obviously, as the Mo$_2$C was increased ($1 \rightarrow 3 \rightarrow 5$ mass%), the content of the α-phase gradually decreased ($52.30 \rightarrow 38.24 \rightarrow 32.5\%$), while the content of β-phase was significantly increased ($45.42 \rightarrow 48.03 \rightarrow 50.81\%$). Moreover, the TiC phase also increased rapidly ($0.68 \rightarrow 8.93 \rightarrow 15.21\%$). In other words, with the increased amount of added Mo$_2$C, the α-phase gradually decreased, while the β-phase and TiC phase gradually increased. This result is coherent with the previous discussion and studies in this paper.

TABLE 2

EBSD analysis of the structure distribution ratio for Ti-8Nb-4Co-xMo$_2$C alloys after sintering at 1300°C for 1 h

	Phase Name	**α-Ti**	**β-Ti**	**TiC**	**Zero**
1 Mo$_2$C Hit Rate 98.40%		52.30	45.42	0.68	1.60
3 Mo$_2$C Hit Rate 95.19%	Phase Fraction (%)	38.24	48.03	8.93	4.81
5 Mo$_2$C Hit Rate 98.37%		32.35	50.81	15.21	1.63

The EPMA and EBSD analyses of the different additions of Mo$_2$C show similar results. Subsequently, taking the 1300°C sintered- 3 Mo$_2$C (Ti-8Nb-4Co-3Mo$_2$C) specimens as an example, Fig. 8 displays the EPMA analysis of the element distributions for the 3 Mo$_2$C specimens after sintering at 1300°C for 1 h. It can be seen from the BEI image that the β-phase should contain more elements that are larger than the atomic weight of titanium (such as Nb, Co, and Mo). It is reasonable to suggest that the bright area is the β-phase and the gray area is the α-phase. Meanwhile, the carbon element is mainly concentrated in the carbides of the black particles, as shown in Fig. 8a. In addition, this study found that Ti was distributed in the α-phase, the β-phase, or the carbides, meaning the area with higher concentration is mainly where the α-phase is located, as shown in Fig. 8b. Generally speaking, as the β-phase in the grain inhibited the precipitation of the α-phase during the cooling process, it led to the refinement of the structure. In this study, the Co and Mo elements obviously tended to be distributed in the β-phase region, which has the effect of strengthening the Ti-8Nb-4Co-xMo$_2$C alloys, as shown in Figs. 8d and 8e. Compared with other elements, it can be
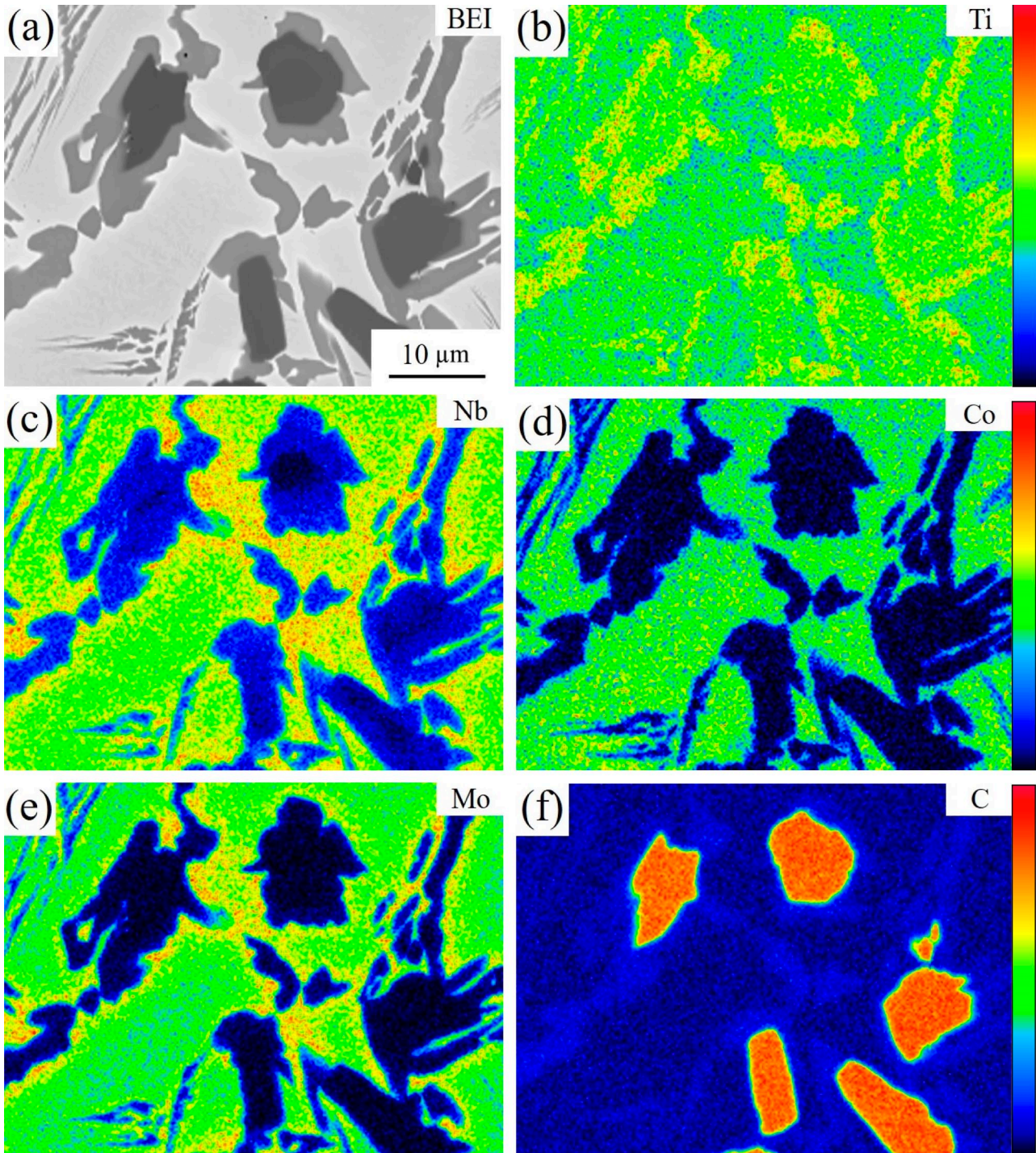

Fig. 8. EPMA-Mapping analysis of the elements distribution for Ti-8Nb-4Co-3Mo$_2$C alloys after sintering at 1300°C for 1 h: (a) BEI image, (b) Ti, (c) Nb, (d) Co, (e) Mo, and (f) C

observed that Ti and a small amount of Nb are also distributed in the area where the C element is located; thus, it is reasonably inferred that the black particles (Fig. 8a) are TiC carbides. At the same time, a small amount of the Nb solid-solution around the TiC precipitates was observed, as seen in Figs. 8c and 8f.

Fig. 9 presents the crystal orientation map (COM) of the EBSD analysis for the 1300°C sintered- 3 Mo_2C specimens. As seen in Fig. 9a, the specimen shows that all phases have no specific crystal orientation. Furthermore, it can be found that the slender flaky α-Ti of the HCP structure has the orientation in the three crystal directions of [0001], [$\bar{1}2\bar{1}0$], and [01$\bar{1}0$], respectively, as shown in Fig. 9b, meaning the structure of α-Ti does not have a specific crystal orientation. Fig. 9c shows that the β-Ti of the BCC structure has different color blocks, which is the position of the crystal grain distribution. Moreover, continuous α-phase precipitates appear at the grain boundaries, and there is no specific crystal orientation. In addition, the TiC structure also shows the same result, meaning there is no specific crystal orientation, as shown in Fig. 9d. In other words, none of the precipitates produced under the PM process have directionality. It was observed that, while TiC was mainly distributed on the large carbide particles, the solubility of C in the Ti alloy was only 0.2%, thus, only a small amount of TiC was dispersed in β-Ti. According to the above discussion and results,

the microstructure of vacuum sintering Ti-8Nb-4Co-3Mo_2C alloys possesses both α and β-phase structures, as well as TiC precipitates. Overall, the main strengthening mechanisms of vacuum sintering Ti-8Nb-4Co-xMo_2C alloys include dispersion strengthening, solid-solution strengthening, and precipitation hardening. Moreover, the sintering properties of the Ti-8Nb-4Co alloy were effectively improved by adding a suitable amount of Mo_2C powder *via* the vacuum sintering process.

4. Conclusions

In this study, Ti-8Nb-4Co alloy powders were combined with Mo_2C powders in varying ratios through vacuum sintering of the PM technique, with the aim of improving the alloy's properties. The results showed that adding an appropriate amount of Mo_2C reduced the alloy's porosity and inhibited grain growth, while also enhancing its mechanical properties and corrosion resistance. Specifically, the addition of 3 mass% Mo_2C produced the best results in terms of hardness, transverse rupture strength, and corrosion resistance.

XRD analysis revealed that the sintered Ti-8Nb-4Co-xMo_2C alloys contained α-Ti, β-Ti, and TiC precipitates, while EPMA and EBSD confirmed the absence of specific crystal orienta-
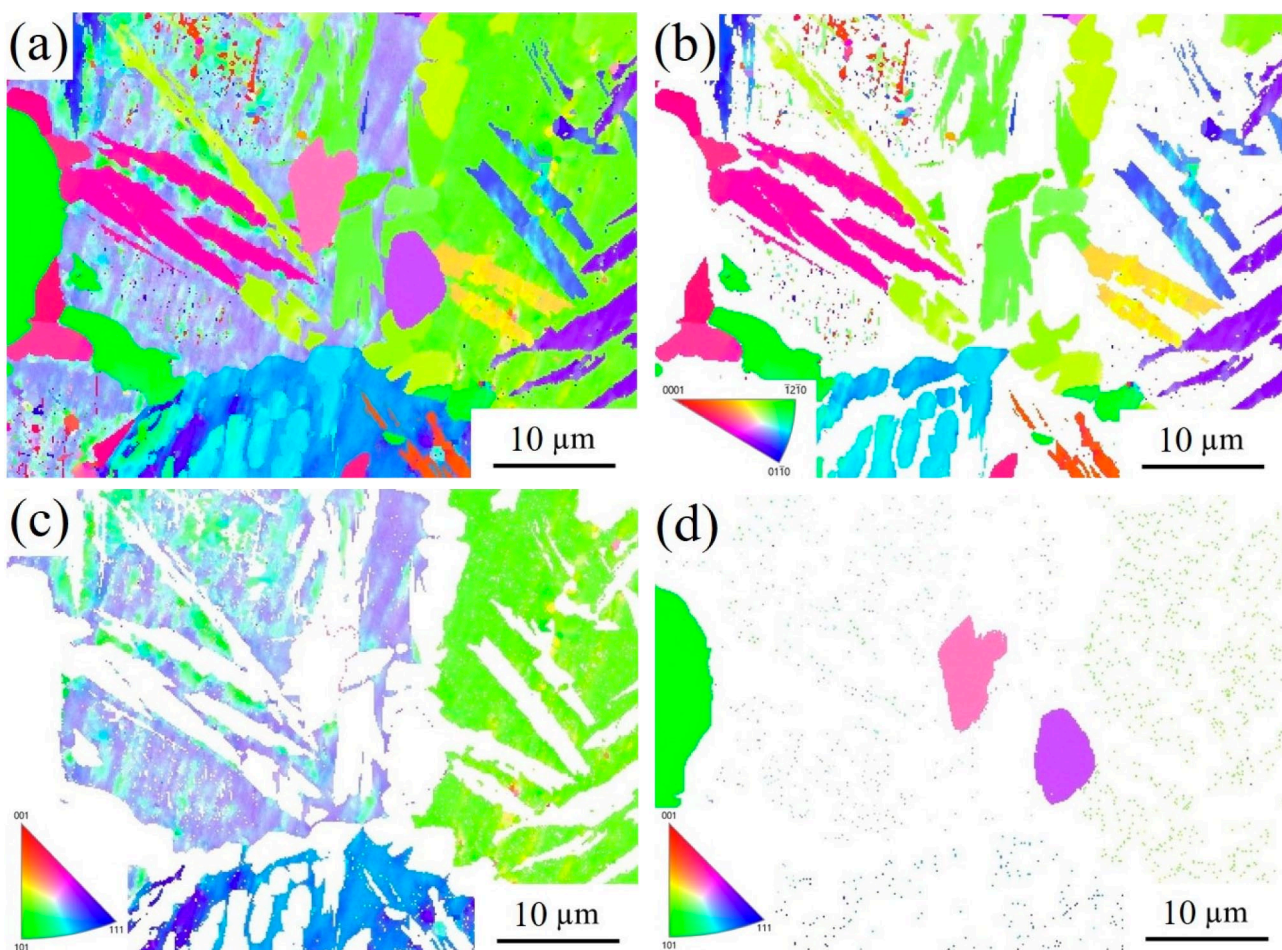

Fig. 9. The crystal orientation map of the EBSD analysis for Ti-8Nb-4Co-3Mo_2C alloys after sintering at 1300°C for 1 h: (a) all phases, (b) α-Ti, (c) β-Ti, and (d) TiC, respectively

tions in these phases. The in situ reduction reaction of $Mo_2C + 2Ti \rightarrow 2TiC + 2Mo$ also occurred during vacuum sintering. The strengthening mechanisms observed in the sintered alloys were dispersion strengthening, solid-solution strengthening, and precipitation hardening.

Overall, these findings demonstrate the potential of using Mo_2C as a reinforcing phase for Ti-8Nb-4Co alloys, and provide insights into the microstructural changes that occur during sintering. Further research is needed to optimize the addition of Mo_2C and explore other reinforcement options, but the results of this study offer a promising starting point for improving the properties of these alloys.

REFERENCE

[1] C.A.F. Salvador, E.L. Maia, F.H. Costa, J.D. Escobar, J.P. Oliveira, Scientific Data **8**, 1-6 (2022).

[2] B. Callegari, J.P. Oliveirac, K. Aristizabal, R.S. Coelho, P.P. Brito, L. Wu, N. Schell, F.A. Soldera, F. Mücklich, H.C. Pinto, Materials Characterization **165**, 110400 (2020).

[3] B. Callegari, J.P. Oliveira, R.S. Coelho, P.P. Brito, N. Schell, F.A. Soldera, F. Mücklich, M.I. Sadik, J.L. García, H.C. Pinto, Materials Characterization **162**, 110180 (2020).

[4] S. Raynova, F. Yang, L. Bolzoni, Materials Science and Engineering: A **799**, 140157 (2021).

[5] C.B. Yi, Y.X. Yuan, L. Zhang, Y.H. Jiang, Z.Y. He, Journal of Alloys and Compounds **879**, 160473 (2021).

[6] I. Çaha, A.C. Alves, P.A.B. Kuroda, C.R. Grandini, A.M.P. Pinto, L.A. Rocha, F. Toptan, Corrosion Science **167**, 108488 (2020).

[7] D. Kalita, Ł. Rogal, T. Czeppe, A. Wójcik, A. Kolano-Burian, P. Zackiewicz, B. Kania, J. Dutkiewicz, Journal of Materials Engineering and Performance **29**, 1445-1452 (2020).

[8] D. Kalita, Ł. Rogal, P. Bobrowski, T. Durejko, T. Czujko, A. Antolak-Dudka, E. Cesari, J. Dutkiewicz, Materials **13**, 2827 (2020).

[9] P.Y. Li, Materials Research Express **6**, 076559 (2019).

[10] B.B. Straumal, A. Korneva, A.R. Kilmametov, L. Lityńska-Dobrzyńska, A.S. Gornakova, R. Chulist, M.I. Karpov, P. Zięba, Materials **12**, 426 (2019).

[11] S.H. Chang, L.Y. Hung, T.H. Yang, Materials Chemistry and Physics **235**, 121743 (2019).

[12] H. Singh, S. Kumar, D. Kumar, Materials Science and Engineering: A **789**, 139577 (2020).

[13] S.H. Chang, C.H. Liang, K.T. Huang, C. Liang, Journal of Alloys and Compounds **857**, 157629 (2021).

[14] S.H. Chang, H.C. Chang, K.T. Huang, Vacuum **187**, 110132 (2021).

[15] S. Cetinkaya, S. Eroglu, JOM **69**, 1997-2002 (2017).

[16] G.H. Zhang, H.Q. Chang, L. Wang, K.C. Chou, International Journal of Minerals, Metallurgy, and Materials **25**, 405-412 (2018).

[17] S.H. Chang, C.Y. Chuang, K.T. Huang, ISIJ International **59**, 1354-1361 (2019).

[18] J. Dang, G.H. Zhang, L. Wang, K.C. Chou, P.C. Pistorius, Journal of the American Ceramic Society **99**, 819-824 (2016).

[19] E Yılmaz, A. Gökçe, F. Findik, O. Gulsoy, O. Iyibilgin, Journal of the Mechanical Behavior of Biomedical Materials **87**, 59-67 (2018).

[20] E Yılmaz, A. Gökçe, F. Findik, O. Gulsoy, Journal of Alloys and Compounds **746**, 301-313, (2018).

[21] E. Yılmaz, A. Gökçe, F. Findik, O. Gulsoy, Journal of Thermal, Analysis and Calorimetry **134**, 7-14, (2018).

[22] E.O. Hall, Proceedings of the Physical Society. Section B **64**, 747-753 (1951).

[23] N.J. Petch, Journal of the Iron and Steel Institute **174**, 25-28 (1953).

[24] S.R. Shatynski, Oxidation of Metals **13**, 105-118 (1979).